We are IntechOpen,
the world's leading publisher of
Open Access books
Built by scientists, for scientists

5,900
Open access books available

145,000
International authors and editors

180M
Downloads

Our authors are among the

154
Countries delivered to

TOP 1%
most cited scientists

12.2%
Contributors from top 500 universities

CLARIVATE ANALYTICS
BOOK CITATION INDEX
INDEXED

WEB OF SCIENCE™

Selection of our books indexed in the Book Citation Index
in Web of Science™ Core Collection (BKCI)

Interested in publishing with us?
Contact book.department@intechopen.com

Numbers displayed above are based on latest data collected.
For more information visit www.intechopen.com

Electromagnetic Characterization of Composite Materials and Microwave Absorbing Modeling

Davide Micheli[1], Carmelo Apollo[1], Roberto Pastore[1],
Ramon Bueno Morles[1], Mario Marchetti[1] and Gabriele Gradoni[2]

[1]*"Sapienza" University of Rome, Astronautic,
Electric and Energetic Engineering Department (DIAEE),*
[2]*University of Maryland, Institute for Research in Electronics and Applied Physics
(IREAP), Paint Branch Drive, College Park, MD*
[1]*Italy*
[2]*USA*

1. Introduction

This book chapter is based on the experimental activities conducted mainly at Sapienza University of Rome: Astronautic, Electric and Energetic Engineering Department in collaboration with University of Maryland, Institute for Research in Electronics and Applied Physics (IREAP). A branch of scientific research about composite materials is focused on electromagnetic characterization and subsequent application of electric conductive polymers. The use of such structures is relevant in aerospace/aeronautics, for electromagnetic (EM) protection from natural phenomena (lightning), and intentional interference with radar absorbing materials (RAM), in nuclear physics for shields adopted in particle accelerators, and for nuclear EM pulses (NEMP) protection, in electromagnetic compatibility (EMC) for equipment-level shielding, high-intensity radiated fields (HIRF) protection, anechoic chambers (for the realizations of wedges and pyramidal arrays), and human exposure mitigation. In this chapter, composite reinforced by carbon *nanostructured* materials are considered, mainly because of their interesting electromagnetic characteristics, such as *high* electrical conductivity and *excellent* microwave absorption. Composite materials as well their absorption capability are analyzed and numerical design of wide frequency band microwave absorbing structures is presented and discussed in details. It is crucial to highlight the need of interdisciplinary research fields to go through nanomaterials: besides nanotechnology, also electromagnetic wave propagation theory, composite materials manufacturing techniques, evolutionary computation algorithms, and use those to design the "quasi perfect absorber" are strongly required. In particular, we propose an inhomogeneous multilayer absorber made of micrometric graphite (at different wt%), and nanometric carbon particles (SWCNTs, MWCNTs, CNFs, at different wt%). At the end, an improvement of the traditional absorbers has been achieved upon optimization through an in-house winning particle optimization (WPO) algorithm, this last appositely conceived for absorbers optimization. Main goal of the presented work is to optimize the absorbers

achieving lower values (< -10 dB) of both reflection and transmission coefficients for angular apertures within 40° of the impinging plane wave (general far-field approximation of whatever active source). The developed evolutionary computation code is flexible in the selection of the algorithm parameters such as frequency band, incidence angular range, overall maximum multilayer thickness, composite material type of each layer, possibility to decide if the design optimization procedure must privilege thickness minimization and/or microwave absorption maximization during design.

With respect to the present literature, the developed method considers the absorption capability taking into account both the reflection and the transmission properties of the entire multilayer structure. Moreover the absorption properties of the multilayer structures have been analyzed considering oblique incidence at fixed angles within a finite range.

From the above explanation it is easy to understand the importance of numerical techniques such as evolutionary computation to design and optimize the absorber.

Absorber mathematical model described in this chapter have been experimentally validated in laboratory (www.saslab.eu) located in DIAEE at Sapienza University of Rome. At the end of chapter the experimental validation is discussed.

2. Composite materials manufacturing and carbon filler analysis

This section focuses on characterization of nanomaterials adopted to build the electrically conductive composite materials and in nanostructured composite materials manufacturing. In formulating an electrically conductive composite material, a polymer is combined with highly conductive rigid particles. Electrical conductivity is accomplished though a certain level of particle-to-particle contact or close proximity. It is difficult to draw definite conclusions about electrical conductivity since it depends also from electromagnetic solicitation type, i.e., DC or AC current and type of electromagnetic wave propagation i.e., direct contacts electrodes or plane wave incidence on the composite material, [D.Micheli et al.,2010], [Xingcun Colin Tong, 2009], [Z. Ounaiesa et al., 2003]. Many further factors can affect the conductive properties of the filler loaded composite, including filler type, loading level, particle distributions, size, and shape, intrinsic conductivity of filler, process condition plating, and compounding. However, the key factors are particle conductivity, loading level and particle shape. The filler concentration -- i.e., the filler in weight % w.r.t. the polymer -- or the volume loading level of the filler is relevant in the *percolation* regime of the composite -- i.e., the threshold at which the composite changes form an insulator to a conductor.

As the filler loading is increased further and reaches a critical point, the conductive particles contact one another, and a continuous network is established. The sudden and precipitous drop in resistivity is achieved through a generation of a continuous network, which is defined as percolation threshold [Weber, M, & Kamal., 1997]. Once achieved the percolation, a majority of the filler particles are in contact with at least two of their nearest neighbours, thereby forming a continuous chain or network. An electrical charge could then be diffused through the composite via this network without encountering the high-resistance polymer resin. Additional filler loading beyond the percolation threshold does not substantially reduce the resistivity of the composite [Sichel, 1982], the greater the aspect ratio of the particles, the smaller the loading level needed to reach the percolation threshold [D.Micheli et al.,2010]. In addition, the mixing process (dispersion) plays an important role in the percolation and conductivity of the conductive composite material. For instance, increasing

the mixing time and hence the specific energy provided during the mixing process, the homogeneity of the spatial distribution of the conductive particle in the matrix is improved and the errors in composite material dielectric permittivity computation at microwave frequencies are reduced. Composite materials considered in this work are based on epoxy matrix reinforced with several species of carbon nanomaterials. These latter have been chosen taking into account the lowest market prices: the economic aspects, normally neglected in small laboratory applications, are on the contrary important in real applications where the amount of carbon nanopowders fillers could be relatively high. In such scenario a good compromise in terms of cost/performances has been obtained using industrial grade multiwall carbon nanotubes (MWCNTs, about 300 $/kg), graphite micropowder (about 40 $/kg). Carbon nanofibers (CNFs, about 30 $/g) has been mainly considered only in the carbon nanopowders analysis, while low cost MWCNTs and graphite micropowder have been largely adopted in the large multilayer tile manufacturing.

2.1 Carbon filler characterization

Carbon materials and epoxyresin considered in the experiments are:

- Micro Graphite (granular size < 20 μm), bought at SigmaAldrich;
- SWCNTs (Single Wall Carbon Nanotubes), bought at Carbolex (diameter around 1-2 nm, length 5-30 μm); http://www.nanotube-suppliers.com
- CNFs (Carbon NanoFibers), bought at SigmaAldrich (diameter around 75 nm, length 50-100 μm); http://www.sigmaaldrich.com/sigma-aldrich/home.html
- MWCNTs (Multi-Wall Carbon Nanotubes type NANOCYL™ NC7000), bought at NANOCYL (diameter around 9.5 nm, length 1.5 μm, purity 90%) http://www.nanocyl.com
- Epoxy-resin is: Prime™ 20LV(density 1.123 g/cm^3), Hardner(density 0.936 g/cm^3); http://www.gurit.com/

Carbon materials weight ratio (wt%) with respect to the polymer (epoxy-resin) are mainly in the range 0.5-3 wt%. Scanning electron microscope (SEM) analysis has been widely adopted in laboratory using VEGA TESCAN SEM model www.tescan.com. In particular, in Fig. 2.1.1, a), b) pictures of functionalized SWCNTs are shown. Functionalization is used to purify CNTs from impurities due to the manufacturing process of CNTs. This can be also carried out through microwave heating, mainly performed by an electromagnetic cavity where the field homogenization can be efficiently achieved [Prato et al., 2008]. In such a process, *a priori* evaluation of power absorption plays a crucial role in prediction of impurity densities. Comparing dimensions of SWCNTs and MWCNTs, it can be observed about 0.05 μm for SWCNTs average diameters and about 2 μm for MWCNTs average diameters, i.e., such type of MWCNTs are typically 40 times greater then SWCNTs. Also topologies of CNTs network appear different: as a matter of fact MWCNTs are rope-like of bundled MWCNTs. Such agglomerations (joint twisting and wrapping) of MWCNTs constitute a trouble in composite materials manufacturing, because of intrinsic difficulties in dispersing CNTs within epoxy resin matrix – i.e., overcoming physico-chemical bonds.

The individual particles in fact are held together by attraction forces of various physical and chemical nature, including Van Der Waals forces and liquid surface tension. The attraction forces must be overcome in order to deagglomerate and disperse the particles into liquid

media. Sonication is a process where ultrasounds are used to drastically reduce the size of particle agglomerates melting against natural attraction forces. Ultrasonic cavitation generates high shear forces that break particle agglomerates into single dispersed particles.
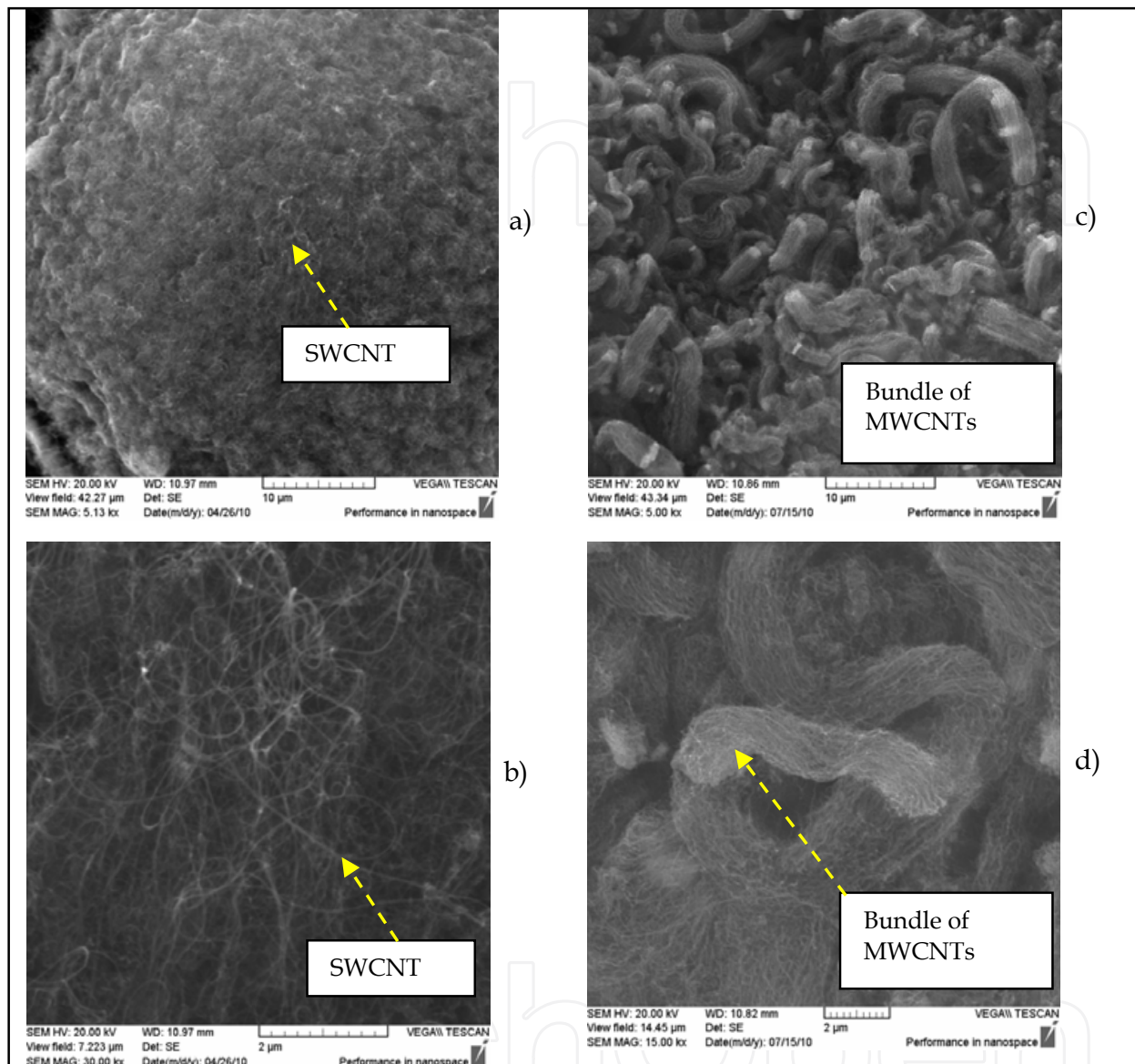

Fig. 2.1.1 a) SWCNTs zoom 5x (10μm scale), b) SWCNTs zoom 30x (2μm scale), c) MWCNTs zoom 5x (10μm scale), d) MWCNTs zoom 15x (2μm scale),

In order to easily compare dimensions of different carbon powders, we report a some picture showing the typical carbon fiber (CF) and carbon nanomaterials we used as SWCNTs MWCNTs and carbon nanofiber (CNFs).

In polymerization process, epoxy-resin tend to spirally wrap CNTs, and if dense CNTs agglomeration takes place the polymerization process sometimes fails and localized parts of composite material could remain in a liquid status without completing the polymerization phase. Such structures are electromagnetically relevant themselves as they might exhibit planar chirality.

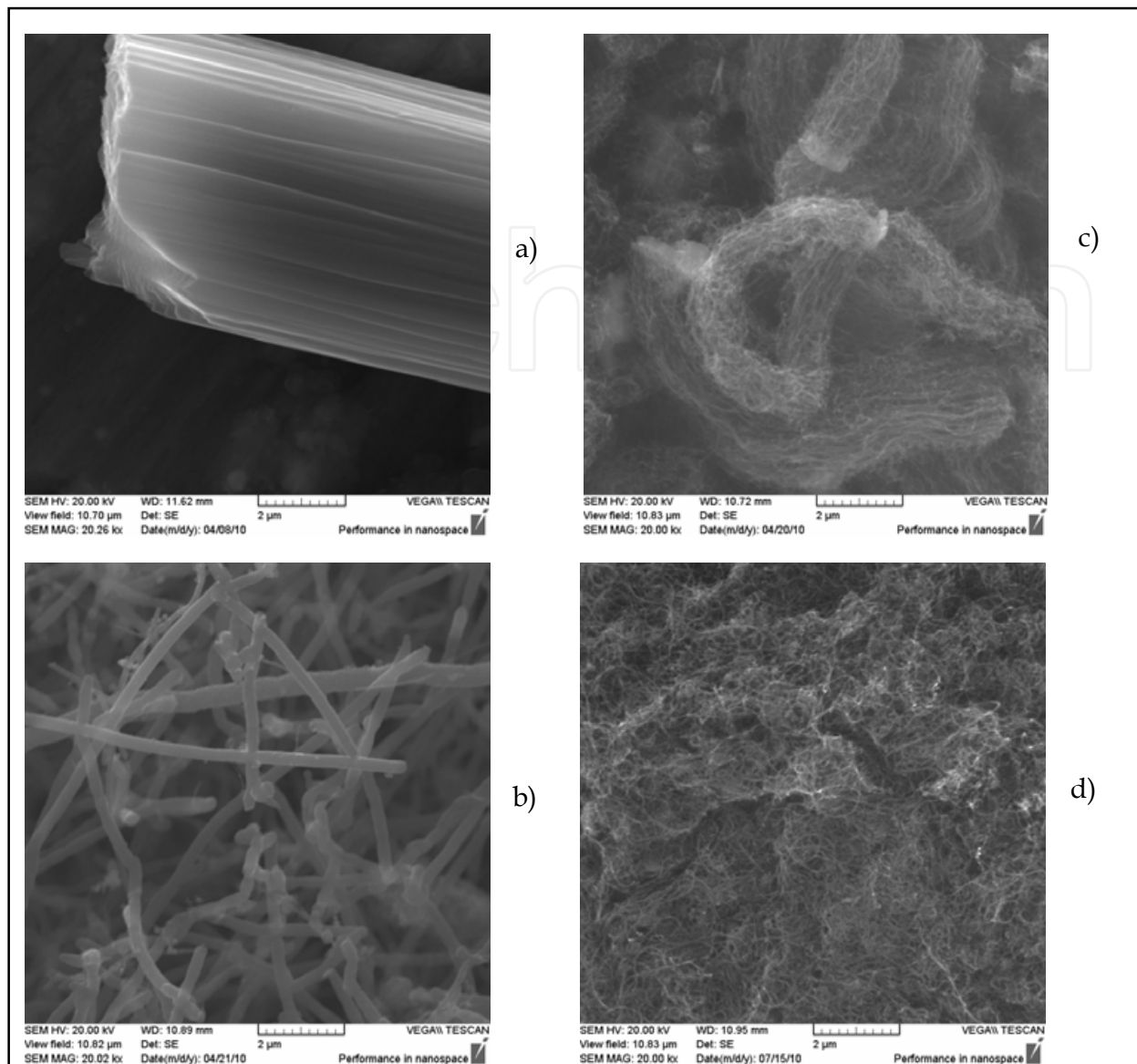This is why we tried to break up MWCNTs by means of sonication.

Fig. 2.1.2. a) Carbon Fiber (CF) zoom 20x (2μm scale), b) Carbon Nanofiber (CNFs) zoom 20x (2μm scale), c) Multi Wall Carbon Nanotube (MWCNTs) zoom 20x (2μm scale), d) Single Wall Carbon Nanotube (SWCNTs) zoom 20x (2μm scale).

2.2 Nanostructured composite material manufactoring

Manufacturing of carbon based nanostrucutred composite materials is achieved through the following steps:

- Eventual carbon powders functionalization.
- Mixing, sonication and degassing of epoxy-resin and carbon nanopowders mixed dispersed with desired weigh percentage;
- Hardener adding, if required by the epoxy-resin;
- Composite curing by oven treatment.

First step is crucial in preparation of homogeneous composite materials. In Fig. 2.2.1, pictures of composite materials preparation are shown. Composite pictures before and a after sonication phase are shown.
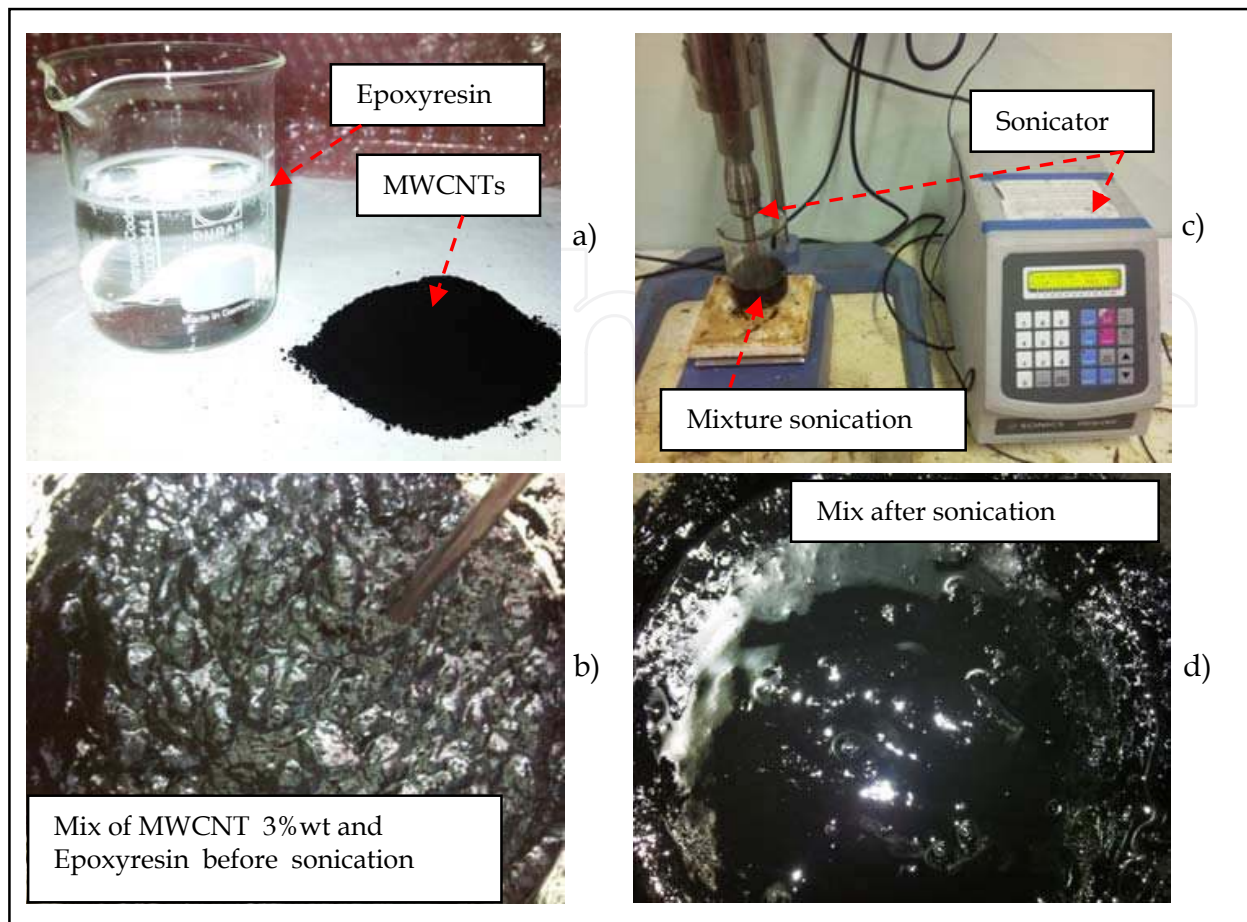
Fig. 2.2.1. a) Ingredients: Epoxyresin and MWCNTs, b) MWCNTs 3%wt and epoxy-resin manually mixed before sonication, c) Sonication process, d) MWCNTs 3%wt and epoxy-resin mixture after sonication.

Observing picture of same composite material before and after sonication phase, immediately appear the difference in the dispersion of MWCNTs.

Nanostructured composite material manufacturing process end up with the injection of described treated liquid mixture in the appropriate sample holder and curing with the appropriate oven treatment. In Fig. 2.2.2., sample holder and oven are shown. In our case, curing process requires about sixteen hours at temperature of 50 C°.

3. Nanostructured composite materials permittivity and microwave absorption characterization

3.1 Microwave measurements

In this section measurement of permittivity of nanostructured composite materials are shown. The microwave characterization process has been carried out by performing scattering parameter measurements and extracting the complex electrical permittivity through canonical algorithms. In particular, we performed the permittivity retrieval by using different algorithms and comparing produced results. The algorithms adopted are Nicholson-Ross, NIST iterative, and non-iterative [L. F.Chen & C. K. Ong, 2004], [Abdel-Hakim & Boughriet, 1997], [James Baker-Jarvis, 1990]. The so obtained results can be
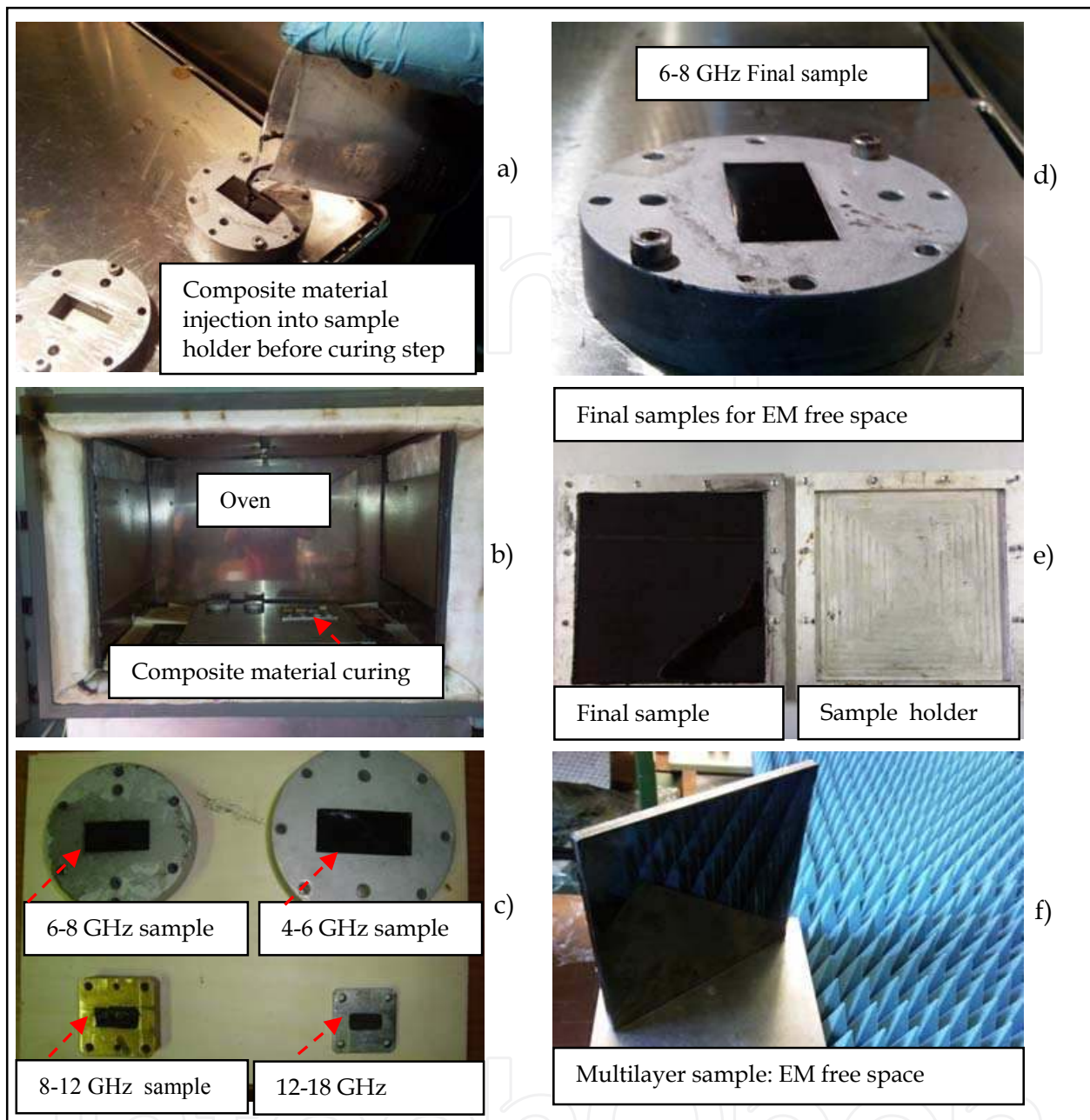
Fig. 2.2.2. a) Injection of liquid composite materials into sample-holder; b) Oven treatment: 16 hours and 50 C°; c,d) Final sample within sample holders for wave guide measurement of electromagnetic properties of composite materials in the band 4-18 GHz ; e,f) 200x200 mm tiles of composite materials for free space electromagnetic absorbing measurements.

considered accurate within the limit of the employed numerical methods. Microwave scattering parameters S_{ij}, with i,j = 1,2, [Davide M. Pozar, 2005], are measured using a Vector Network Analyzer (N5230C Agilent PNA-L) in the waveguide method shown in Fig.3.1.1. Wave guide calibration kit are in the J-band (5.38-8.18 GHz)), X-band (8.2-12.4 GHz), P-band (12.4-18 GHz). Sample holders, hosting the materials under test (MUT), were built using as a shape model the thru connections of Flann and Agilent calibration kits (www.flann.com, www.agilent.com).
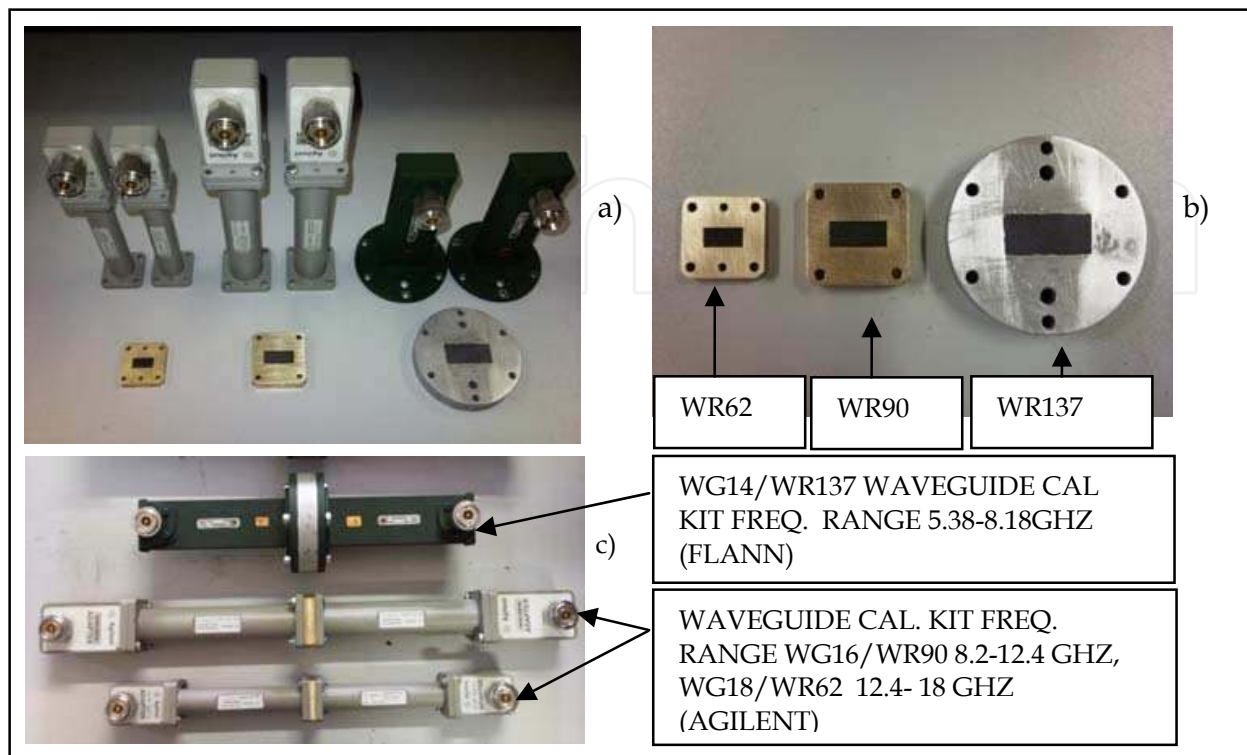
Fig. 3.1.1. a,b,c) Waveguide sections and sample holders covering 5.3 to 18 GHz frequency band.

Scattering parameters connect the input and output circuit quantities using the reflection and transmission parameters normally adopted in microwave analysis. By means of such parameters it is possible to determine the real and the imaginary part of the electrical permittivity and magnetic permeability. All materials have some response to magnetic fields but, except for ferromagnetic and ferromagnetic types, their responses are usually very small, and their permeability values differ from μ_0 by a negligible fraction. In our experiment the relative magnetic permeability is that of free space ($\mu_r = 1$) since no ferromagnetic materials are involved.

The entire frequency-band has been divided in 1536 frequency steps (start 5.38 GHz, end 18 GHz) and, for each one, the corresponding electrical permittivity has been computed. Composite materials based on different weight percentage of carbon nanopowders with respect to the epoxyresin have been analyzed. In particular 0.5, 1, 2, 2.5, 3 %wt for MWCNTs based composite materials and 1, 2, 3wt.% for CNFs based composite materials.

Observing Fig.3.1.2, it can be noticed that the higher the filler weight percentage, the greater both the real and imaginary part of permittivity. This can be ascribed to the electric conductive characteristic of the carbon powders inserted into the epoxy matrix [D.Micheli et al., 2010].

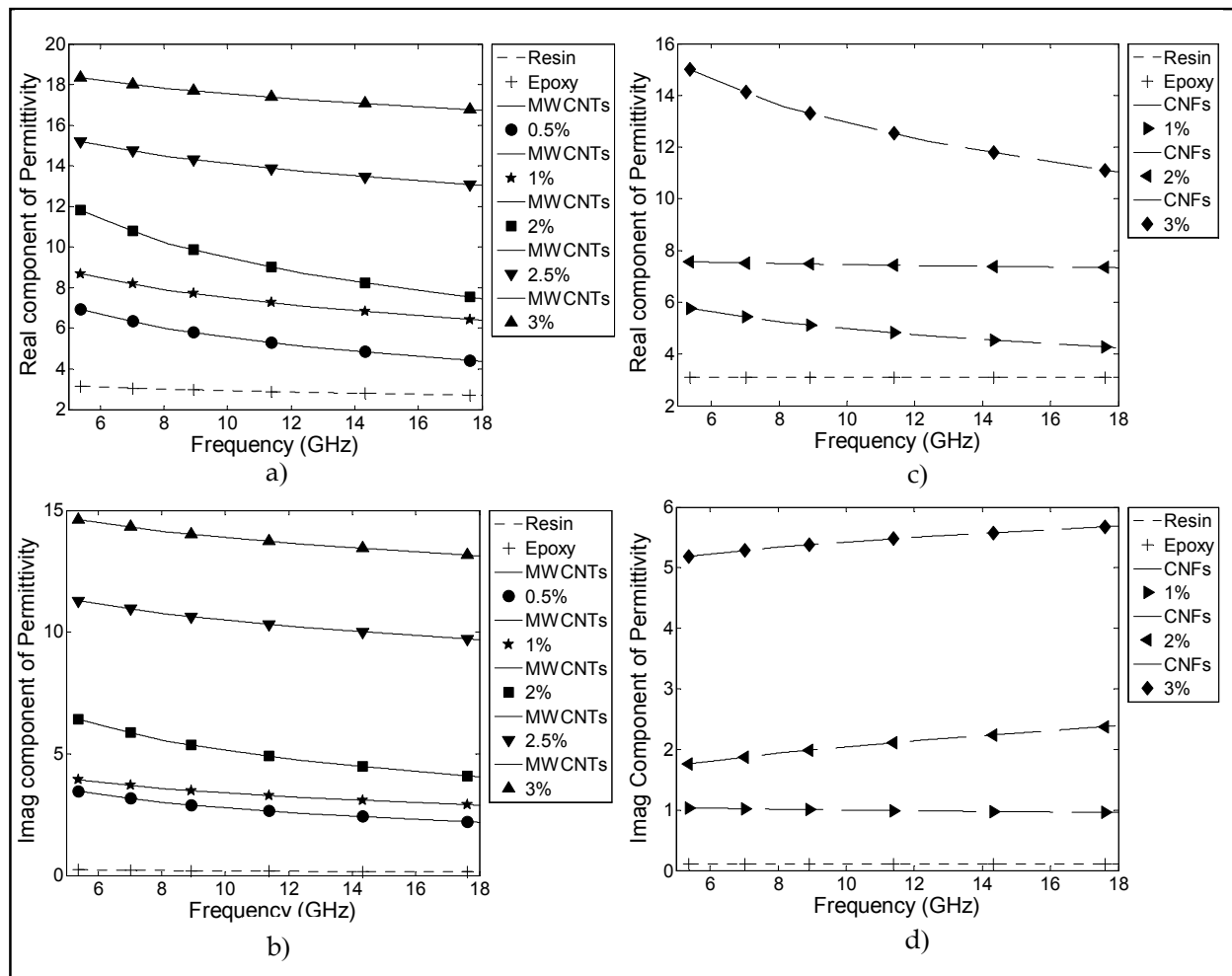In the next section the analysis of materials in terms of electric losses is made.

Fig. 3.1.2. a) Real component; b) Imaginary component of permittivity of nanostructured composite materials based on MWCNTs; c) Real component; b) Imaginary component of permittivity of nanostructured composite materials based on CNFs in the 5.3 to 18 GHz frequency band.

3.2 Microwave electric conductivity

Microwave electrical conductivity of a dielectric material can be evaluated by using the following equation:

$$\varepsilon_r'' = \frac{\sigma}{\omega \varepsilon_0} = \frac{\sigma}{2\pi f \varepsilon_0} \ \Rightarrow \ \sigma(S/m)) = 2\pi f \varepsilon_0 \varepsilon'' \tag{3.2.1}$$

Where σ is the electric conductivity (S/m), ε_0 is the free space permittivity (8.854 × 1E-12 F/m), f is the frequency (Hz), ε'' is the imaginary component of permittivity.

In Fig. 3.2.1, electric conductivity of nanostructured composite materials is reported as function of frequency.

In general, the electric conductivity of nanopowder reinforced composite materials is mainly due to a couple of effects: the first is the high number of inter-nanostructure connections which plays a role in ohmic resistivity reduction, the second is explainable by thinking to the reinforced matrix as a nanocapacitance network, where a single capacitor is constituted

by two faced nanoparticles. The former effect is trivially related to the concentration, and becomes dominant above the percolation threshold, when many conduction pathways cross the matrix thus forming electrical connections. The latter is to be ascribed to the very large nanoparticles specific surface area (A) compared to micro-sized powder: the resulting effective capacitance (C) lowers the composite characteristic impedance, as clear from the fundamental capacitance impedance equation,
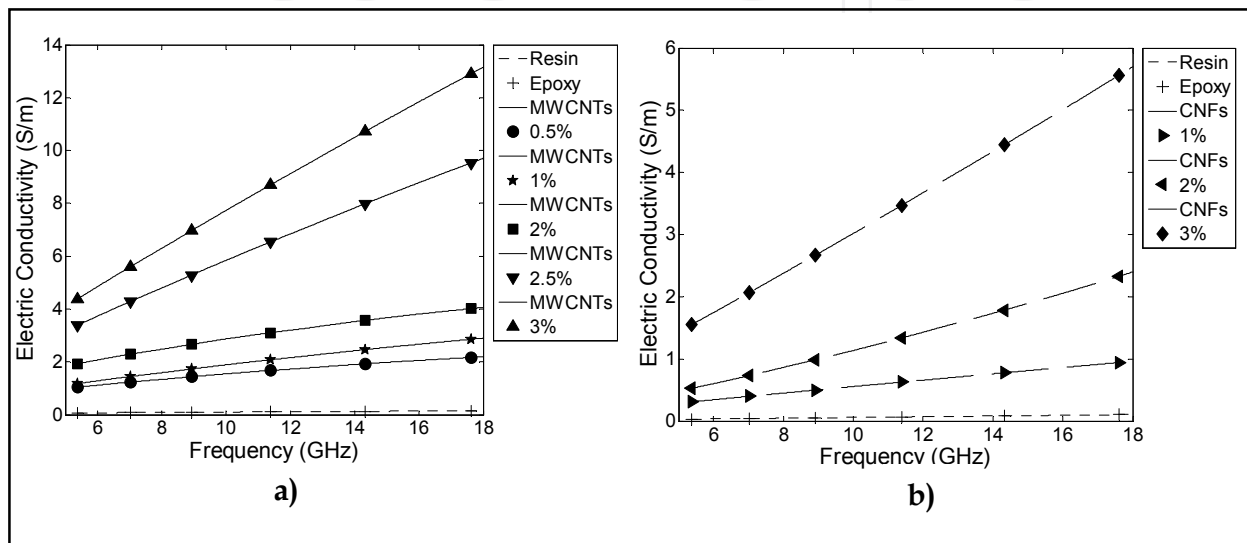
$$Z_C = \frac{1}{j\omega C}$$ (3.2.2)

(where C ∝ A).

Fig. 3.2.2. a) Electric Conductivity (S/m) of MWCNTs based composite materials; b) Electric Conductivity (S/m) of CNFs based composite materials.

3.3 Microwave absorption properties related to impedance matching conditions

From permittivity results, the intrinsic wave impedances of the k-th material can be computed using the following equation.

$$\eta_k = \sqrt{\frac{\mu_0}{\varepsilon_0}} \sqrt{\frac{\mu_{rk}}{\varepsilon_{rk}}} = \sqrt{\frac{\mu_0}{\varepsilon_0}} \sqrt{\frac{\mu_{rk}}{\varepsilon'_{rk} - j\varepsilon''_{rk}}}$$ (3.3.1)

Where μ_{rk} is the relative permeability of the composite (equal to 1), ε_{rk} is the relative permittivity of the composite which is function of the frequency. Intrinsic wave impedance is a complex number and magnitudes are reported in Fig. 3.3.1.

Observing the intrinsic wave impedance plot, it is possible to note that the higher the weight concentration of carbon nanopowders, the lower the intrinsic wave impedance of composite material. As shown in [D.Micheli et al.,2010], the wave impedance plays an important role in microwave reflection and absorption properties of materials in free space propagation condition, in the next section absorbing effectiveness of materials is described.

There are three conditions that can minimize the EMI reflection from a surface. When an electromagnetic wave, propagating through a free space with impedance of Z_0, happens upon a semi-infinite dielectric material boundary of impedance Zi, a partial reflection
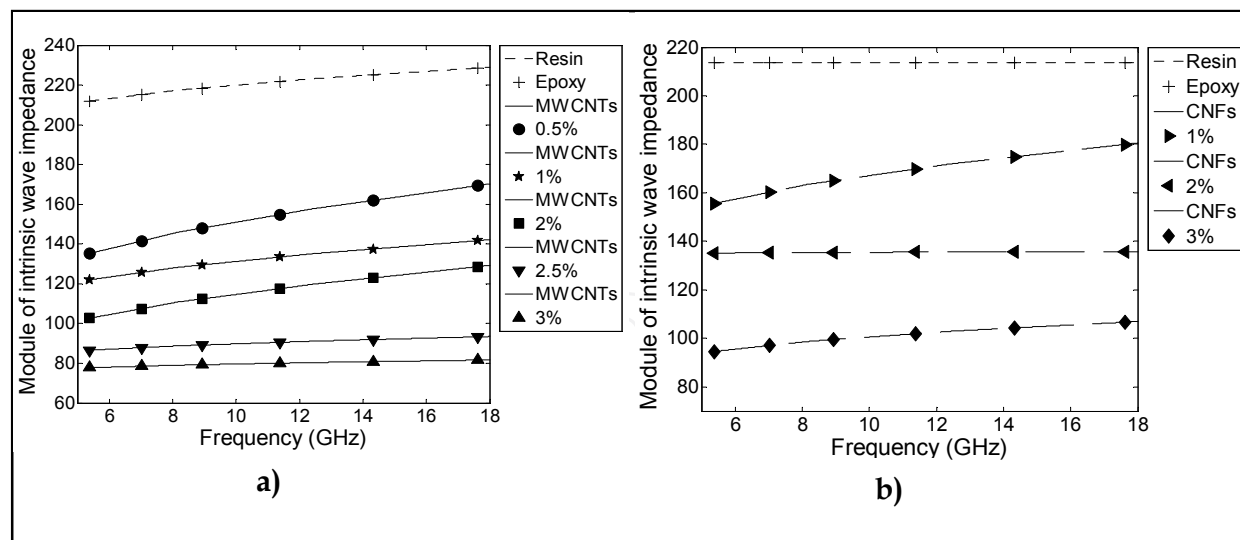
Fig. 3.3.1. a) Intrinsic wave impedance of nanostructured composite materials based on MWCNTs in the 5.3 to 18 GHz frequency band; b) Intrinsic wave impedance of nanostructured composite materials based on CNFs in the 5.3 to 18 GHz frequency band

occurs. The reflection coefficient (dB), at the interface can be expressed using formalism of transmission lines [S. Ramo, J. Whinnery & T. Van Duzer, 1994]:

$$RC(f) = 20Log_{10}\left|\frac{(Z_i - Z_0)}{Z_i + Z_0}\right|$$

(3.3.2)

Where:
RC = Reflection Coefficient (dB);
$Z_0 \sim 377$ (Ω) is the free space impedance;
Z_i=Input impedance at the Air-Absorber interface;
f = frequency (Hz).
The reflection coefficient falls to -∞ when $Z_i=Z_0$, or, in other words, the composite material layer is impedance matched to the incident medium.
Therefore, the absorbing material must be lossy (second condition), so that the EMI energy can be dissipated within the material and impedance matched (first condition), so that the electromagnetic wave is not reflected back. But in order to get a large amount of attenuation, values of permeability and/or permittivity should be large; this condition could imply low values of intrinsic impedance and as a consequence large values of RC(dB). As a consequence design of an absorber is a compromise between the front-face reflection coefficient and the loss per unit thickness. One method to search for the best compromise within the largest frequency band is the multilayer structure. Here the optimization of material of each layer and its related thickness play an important role in absorption maximization.
Some of these structures are characterized by a surface impedance Zi, close as possible to free-space impedance (~377Ω), and then changing their intrinsic impedance inside by gradually increasing their conductivity to keep the reflection coefficient at the boundary of each layer as low as possible, and allow the materials to convert the EMI energy into Joule heating for dissipating. There are a variety of absorbers but they can be classified into two basic types of structures and materials: resonant or graded dielectric or both of them.

In the next section a new search algorithms and absorbers design method are deeply analyzed. The third condition to obtain an absorber can be easily understood rewriting equation of reflection coefficient:

$$RC(f) = 20Log_{10}\left|\frac{(Z_i - Z_0)}{Z_i + Z_0}\right| = 20Log_{10}\left|\frac{\left(\frac{Z_i}{Z_0} - 1\right)}{\left(\frac{Z_i}{Z_0} + 1\right)}\right| \qquad (3.3.3)$$

$$if \quad \mu_{rk} = \varepsilon_{rk} \quad \Rightarrow \quad \frac{Z_i}{Z_0} = \frac{\sqrt{\frac{\mu_0}{\varepsilon_0}}\sqrt{\frac{\mu_{rk}}{\varepsilon_{rk}}}}{\sqrt{\frac{\mu_0}{\varepsilon_0}}} = \sqrt{\frac{\mu_{rk}}{\varepsilon_{rk}}} = 1 \quad \Rightarrow \quad RC(dB) \to -\infty \qquad (3.3.4)$$

In other words when relative permittivity is close to relative permeability values then, the material intrinsic impedance become close to free space impedance (377 Ω) and reflection of electromagnetic wave become very low.

4. Numerical design and optimization of microwave absorber

4.1 Introduction

This Section describes the approach adopted to design and optimize the microwave absorber multilayer structure. First the design and optimization problem are introduced and the electromagnetic model of absorber is described, then, winning particle optimization (WPO) method, are analyzed and applied for the numerical design of the microwave absorber.

Two kind of structures are designed, one explicitly required in microwave absorbing materials (MAM), the other in microwave shielding structures (MSS).

The first commonly called radar absorbing materials (RAM) are mostly known for their applications in stealth fighters and anechoic chambers; the second is developed for enhanced shielding applications where requirements are simultaneously both: microwave shielding and microwave absorbing capability of materials.

Electromagnetic Interference (EMI), defined by NATO as an electromagnetic disturbance which interrupts, obstructs, or otherwise degrades the effective performance of electronic or electrical equipment. In aircraft, EMI can affect everything from fly-by-wire flight control systems to a cockpit fuel gauge and in extreme cases put a plane into an uncommanded dive or shut down a critical avionic system.

Naturally occurring radio noise originating from atmospheric disturbances (including lightning) and extraterrestrial sources (such as sunspots) can also degrade the performance of electronic equipment. Communications signals may also interfere with the operation of sensitive electronic equipment. The most common type of EMI occurs in the radio frequency (RF) range of the electromagnetic (EM) spectrum, from 10^4 to 10^{12} Hertz. This energy can be radiated by computer circuits, radio transmitters, fluorescent lamps, electric motors, overhead power lines, lightning, and many other sources, and device failures caused by interference—or "noise"—from electromagnetic energy are increasing due to the growing number of products that contain sensitive electronic components. This is why we are

studying structures which simultaneously are able of absorbing and shielding from microwave point of view.

4.2 Electromagnetic model of multilayer absorber

In RAM applications, reflection coefficient (RC) at the first air-multilayer interface can been used as the main objective function (OF) parameter which need to be reduced using numerical optimization techniques, whereas in shielding ones the most stringent requirement considered is the transmission coefficient (TC) lowering. The multilayer absorption is a key feature in shielding applications too, because of evident protection constraints, so it has been quantified through the so-called 'loss factor' (LF%), defined as [D.Micheli et, al,. 2009], and [D.M.Pozar, 2005]:

$$LF\% = \left(1 - |RC|^2 - |TC|^2\right) \cdot 100 \tag{4.2.1}$$

Where:
RC is the Reflection Coefficient expressed in the linear form.
TC is the Transmission Coefficient expressed in the linear form.
Its physical meaning is related to the fraction of the incident power vanishing inside the materials due to localization and dissipation phenomena. Since the calculation of RC and TC becomes a crucial point for the optimization goal, a rigorous approach to relate transmitted and reflected waves to the incident one inside each layer has been adopted. In particular, such theoretical model relies on the forward/backward propagation matrix formalism introduced in chapter one, accounting for each single interface effect on the local field crossing. Both normal and oblique incidences have been evaluated during the automatic optimization. Numerical optimization require the definition of some boundary conditions for the dimensions of the multilayer structure adopted as absorber model [D.Micheli et, al,. 2010]. For all absorber presented in this book the thickness of each layer can range from 0 up to 3 mm. Number of layers of absorber is upper-limited to maximum ten layers. The effective number of layers is established each time by the numerical optimization procedure which is able to remove one or more layers of the multilayer structure. Multilayer configuration structures are depicted in Fig. 4.2.1.

It could be noticed that last layer could be air (i.e. free space in this context), or a perfect electric conductor (PEC) as a function of the absorber we are interested to optimize. Usually in typically RAM application PEC is applied since is assumed that such absorber need to be applied like a coating on an existing metal based structure like an airplane or a boat. On the contrary, in shielding application air is usually assumed as the surrounding medium for the absorber.

The design algorithm needs to be capable not only to choose the number of layers and their thickness but the material type too. In other words in the multilayer structure, layers order is not a priori fixed but numerical techniques decides completely all layers parameters, from layers number and layer thicknesses up to best composite material which must be adopted for each layer of the multilayer structure. Without lack of generality, the case of normal incidence is here reported, even though the current implemented formulation takes account of both TM/TE modes. For an arbitrary layer u of the configuration depicted in Fig.4.2.1 it is possible to write [D.Micheli et, al,. 2010],
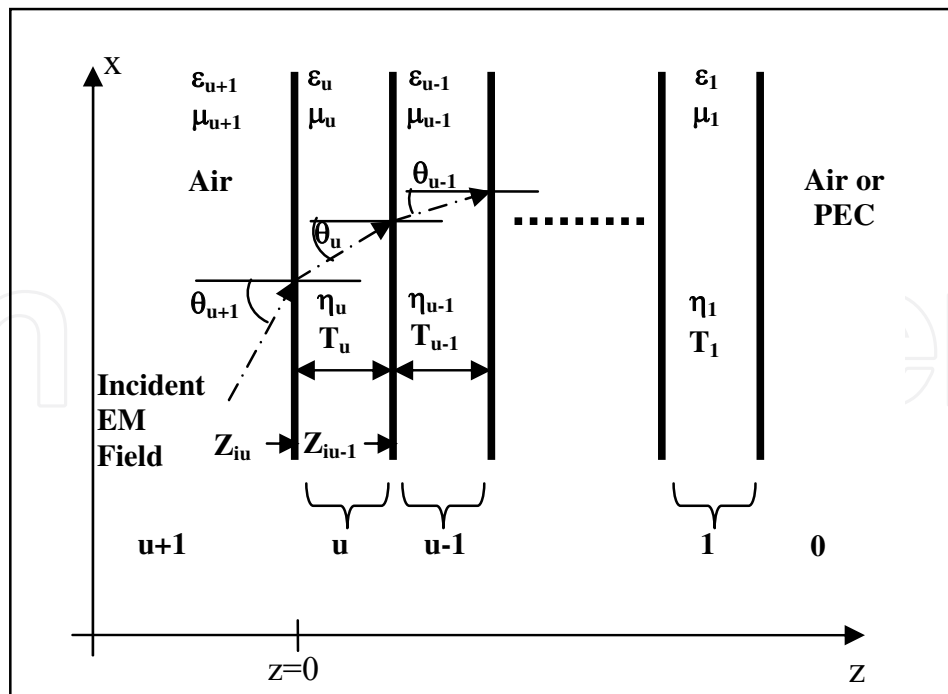
Fig. 4.2.1. General Multilayer scheme.

$$E_u^+ e^{-j\kappa_{uz}z_u} + E_u^- e^{j\kappa_{uz}z_u} = E_{u-1}^+ e^{-j\kappa_{u-1z}z_u} + E_{u-1}^- e^{j\kappa_{(u-1)z}z_u}$$

$$\frac{\eta_{u+1}}{\eta_u} E_u^+ e^{-j\kappa_{uz}z_u} - \frac{\eta_{u+1}}{\eta_u} E_u^- e^{j\kappa_{uz}z_u} = E_{u-1}^+ e^{-j\kappa_{(u-1)z}z_u} - E_{u-1}^- e^{j\kappa_{(u-1)z}z_u}$$

(4.2.1)

now, summing and subtracting each member of Eq. (4.2.1), it is straightforward to obtain

$$\left(1 + \frac{\eta_{u-1}}{\eta_u}\right) E_u^+ e^{-j\kappa_{uz}z_u} + \left(1 - \frac{\eta_{u-1}}{\eta_u}\right) E_u^- e^{j\kappa_{uz}z_u} = 2E_{u-1}^+ e^{-j\kappa_{(u-1)z}z_u}$$

$$\left(1 - \frac{\eta_{u-1}}{\eta_u}\right) E_u^+ e^{-j\kappa_{uz}z_u} + \left(1 + \frac{\eta_{u-1}}{\eta_u}\right) E_u^- e^{j\kappa_{uz}z_u} = 2E_{u-1}^- e^{j\kappa_{(u-1)z}z_u}$$

(4.2.2)

In order to establish a clear relationship between fields in u-th and (u-1)-th layers, upon multiplication of $e^{-j\kappa_{u-1}(z_{u-1}-z_u)}$ by the first of (4.2.1), and by the second of (4.2.1), we obtain

$$\frac{1}{2}\left(1 + \frac{\eta_{u-1}}{\eta_u}\right) E_u^+ e^{-jk_{uz}z_u} e^{-jk_{(u-1)z}(z_{u-1}-z_u)} + \frac{1}{2}\left(1 - \frac{\eta_{u-1}}{\eta_u}\right) E_u^- e^{+jk_{uz}z_u} e^{-jk_{(u-1)z}(z_{u-1}-z_u)} =$$

$$= E_{u-1}^+ e^{-jk_{(u-1)z}z_{u-1}}$$

(4.2.3)

$$\frac{1}{2}\left(1 - \frac{\eta_{u-1}}{\eta_u}\right) E_u^+ e^{-jk_uz_u} e^{+jk_{(u-1)z}(z_{u-1}-z_u)} + \frac{1}{2}\left(1 + \frac{\eta_{u-1}}{\eta_u}\right) E_u^- e^{+jk_uz_u} e^{+jk_{(u-1)z}(z_{u-1}-z_u)} =$$

$$= E_{u-1}^- e^{+jk_{(u-1)z}z_{u-1}}$$

(4.2.4)

Then, considering field and propagator products with common subscripts and taking advantage of the matrix formalism, one gets

$$\begin{bmatrix} E_{u-1}^+ e^{-jk_{(u-1)z}z_{u-1}} \\ E_{u-1}^- e^{+jk_{(u-1)z}z_{u-1}} \end{bmatrix} = \overline{\overline{V_{(u-1),u}}} \cdot \begin{bmatrix} E_u^+ e^{-jk_{uz}z_u} \\ E_u^- e^{+jk_{uz}z_u} \end{bmatrix} \tag{4.2.5}$$

Where: $$R_{(u-1),u} = \dfrac{\left(1 - \dfrac{\eta_{u-1}}{\eta_u}\right)}{\left(1 + \dfrac{\eta_{u-1}}{\eta_u}\right)} = \dfrac{\eta_u - \eta_{u-1}}{\eta_u + \eta_{u-1}} \tag{4.2.6}$$

And:
$$\overline{\overline{V_{(u-1),u}}} = \frac{1}{2}\left(1 + \frac{\eta_{u-1}}{\eta_u}\right)\begin{bmatrix} e^{-jk_{(u-1)z}(z_{u-1}-z_u)} & R_{(u-1),u}e^{-jk_{(u-1)z}(z_{u-1}-z_u)} \\ R_{(u-1),u}e^{+jk_{(u-1)z}(z_{u-1}-z_u)} & e^{+jk_{(u-1)z}(z_{u-1}-z_u)} \end{bmatrix} =$$
$$= T_u^{-1}\begin{bmatrix} e^{-jk_{(u-1)z}(z_{u-1}-z_u)} & R_{(u-1),u}e^{-jk_{(u-1)z}(z_{u-1}-z_u)} \\ R_{(u-1),u}e^{+jk_{(u-1)z}(z_{u-1}-z_u)} & e^{+jk_{(u-1)z}(z_{u-1}-z_u)} \end{bmatrix} \tag{4.2.7}$$

In (4.2.5) the 'local' transmission coefficient takes the usual form

$$T_u = \frac{2\eta_u}{\eta_u + \eta_{u-1}} \tag{4.2.8}$$

as well as the 'local' reflection coefficient:

$$R_{u-1} = \frac{\eta_{u-1} - \eta_u}{\eta_{u-1} + \eta_u} \tag{4.2.9}$$

Both the expressions involve the intrinsic layer impedances η. Each matrix element of (4.2.5) models the *(u-1)*-th layer crossing through the phase shift

$$\delta_{u-1} = k_{(u-1)z}(z_{u-1} - z_u) = k_{(u-1)z}d_{u-1} \tag{4.2.10}$$

Where $k_{(u-1)z}$ and d_{u-1} are the layer wavenumber along z-axes and layer thickness respectively.

Following the above formalism, the overall multilayer reflection and transmission can be calculated through the simple matrix product:

$$\overline{\overline{V_{0,n}}} = \overline{\overline{V_{0,1}}} \cdot \overline{\overline{V_{1,2}}} \cdots \cdots \overline{\overline{V_{n-1,n}}} \tag{4.2.11}$$

Each <u>matrix</u> represents a material interface. In particular $\overline{\overline{V_{0,1}}}$ is referred to last interface while $\overline{\overline{V_{n-1,n}}}$ is referred to the initial free-space and layer material interface met by the propagating electromagnetic wave.

Referring to (4.2.1), it is worth noticing that the number of material strata is exactly (n+1) - i.e., the number of interfaces plus one required to take into account the interface between last layer of the multilayer and the surrounding theoretically infinite medium (free space or PEC).

Now let us to consider the interface separating the last two regions *n* and *n-1*, in case of right-hand unbounded medium (often called as the multilayer coating) where the last-th layer is air we get for the last interface:

$$\begin{bmatrix} E_n^+ e^{-jk_t z_n} \\ E_n^- e^{+jk_{t1} z_n} \end{bmatrix} = \frac{1}{2}\left(1 + \frac{\eta_n}{\eta_{n-1}}\right) \cdot \begin{bmatrix} 1 & R_{n,n-1} \\ R_{n,n-1} & 1 \end{bmatrix} \cdot \begin{bmatrix} E_{n-1}^+ e^{-jk_{n-1} z_{n-1}} \\ E_{n-1}^- e^{+jk_{n-1} z_{n-1}} \end{bmatrix} \qquad (4.2.12)$$

Where:

$$\overline{\overline{V_{n,n-1}}} = \frac{1}{2}\left(1 + \frac{\eta_n}{\eta_{n-1}}\right) \cdot \begin{bmatrix} 1 & R_{n,n-1} \\ R_{n,n-1} & 1 \end{bmatrix} =$$
$$= T_{n-1}^{-1} \begin{bmatrix} 1 & R_{n,n-1} \\ R_{n,n-1} & 1 \end{bmatrix} \qquad (4.2.13)$$
$$\Downarrow$$

since in our scenario $n = 1$ and $n - 1 = 0$ we have:

$$\overline{\overline{V_{1,0}}} = T_0^{-1} \begin{bmatrix} 1 & R_1 \\ R_1 & 1 \end{bmatrix}$$

Which gains symmetry and anti-symmetry properties, whereas in the case of a perfect electrical conductor (PEC) backed absorber, we find the unitary matrix:

$$\overline{\overline{V_{1,0}}} = \begin{bmatrix} 1 & 1 \\ 1 & 1 \end{bmatrix} \qquad (4.2.14)$$

Such a simplified forms is not retrievable from (4.2.7) directly, hence the application of boundary conditions is further required in deriving it. Once calculated the general matrix of (4.2.11) one can relate the fields impinging from unbounded left-hand medium to the field outgoing from the last interface. In case of unbounded right-hand medium, we obtain

$$\begin{pmatrix} E_n^+ \\ 0 \end{pmatrix} = \overline{\overline{V_{n,0}}} \cdot \begin{pmatrix} E_0^+ \\ E_0^- \end{pmatrix} \quad \text{i.e.,} \quad \begin{pmatrix} E_n^+ \\ 0 \end{pmatrix} = \begin{bmatrix} V_{n,0}^{1,1} & V_{n,0}^{1,2} \\ V_{n,0}^{2,1} & V_{n,0}^{2,2} \end{bmatrix} \cdot \begin{pmatrix} E_0^+ \\ E_0^- \end{pmatrix} \qquad (4.2.15)$$

Whereas in case of PEC medium, Eq. (4.2.15) turns into

$$\begin{pmatrix} 0 \\ 0 \end{pmatrix} = \begin{bmatrix} V_{n,0}^{1,1} & V_{n,0}^{1,2} \\ V_{n,0}^{2,1} & V_{n,0}^{2,2} \end{bmatrix} \cdot \begin{pmatrix} E_0^+ \\ E_0^- \end{pmatrix} \qquad (4.2.16)$$

Drawing on representation of (4.2.22) or (4.2.23) it's straightforward to find a formal expression of reflection coefficient Γ at the first interface and of transmission coefficient T. They are defined as

$$\Gamma = \frac{E_0^-}{E_0^+} = -\frac{V_{n,0}^{2,1}}{V_{n,0}^{2,2}} \qquad (4.2.17)$$

$$T = \sqrt{\frac{\eta_0}{\eta_n}} \frac{E_n^+}{E_0^-} = \sqrt{\frac{\eta_0}{\eta_n}}\left(V_{n,0}^{1,1} - V_{n,0}^{1,2} \frac{V_{n,0}^{2,1}}{V_{n,0}^{2,2}}\right) \qquad (4.2.18)$$

As will be discuss later on the chapter, the employed algorithm can operate in different optimization-oriented modalities. The one toward the minimization of material thickness needs for the possibility of removing layers from the maximum allowed set. This means that, in bringing optimization, a layer could not be necessary anymore - i.e. no longer physically present - even though related interface matrixes are still required for product completion of (4.2.90). This is easy to figure out in automatic computation contexts: in other words, when an arbitrary layer is removed the u-th thickness $du = z_{u-1} - z_u = 0$ tends to zero and Eq.(4.2.7) turns into the identity matrix:

$$\overline{\overline{V_{(u-1),u}}} = \frac{1}{\dfrac{2\eta_u}{\eta_u + \eta_{u-1}}} \begin{bmatrix} e^{-jk_{(u-1)z}(z_{u-1}-z_u)} & R_{(u-1),u}e^{-jk_{(u-1)z}(z_{u-1}-z_u)} \\ R_{(u-1),u}e^{+jk_{(u-1)z}(z_{u-1}-z_u)} & e^{+jk_{(u-1)z}(z_{u-1}-z_u)} \end{bmatrix} = $$
$$= 1 \cdot \begin{bmatrix} e^{-jk_{(u-1)z}(0)} & R_{(u-1),u}e^{-jk_{(u-1)z}(0)} \\ R_{(u-1),u}e^{+jk_{(u-1)z}(0)} & e^{+jk_{(u-1)z}(0)} \end{bmatrix} = \begin{bmatrix} 1 & 0 \\ 0 & 1 \end{bmatrix}$$

(4.2.19)

In such case we take $\eta_{u-1} = \eta_u$ and $n_{u-1} = n_u$ as a consequence and hence does not affect the crossing field. So, provided this rule is properly applied, matrix of Eq.(4.2.15) Eq.(4.2.15) are the only required for the implementation. One further critical occurrence to be taken into account is that of the last layer removal. If this happens, the last matrix form of (4.2.15) must shift backward to the previous interface of Eq.(4.2.11) and $\overline{\overline{V_{n,n-1}}} = \overline{\overline{I_2}}$; this procedure must be iterated when multiple layers close to the last interface are removed. Such type of check can be executed from the right to the left or vice versa as a function of the initial layer thickness checked at the start of the procedure. Oblique incidence can be easily accounted for upon insertion of TE and TM impedance form in Eq.(4.2.7).

5. Search algorithm adopted to design multilayer absorber

The most popular evolutionary algorithm is Genetic Algorithm (GA). GA attempts to simulate the phenomenon of natural evolution. In natural evolution, each species searches for beneficial adaptations in an ever-changing environment.
As species evolve, the new attributes are encoded in the chromosomes of individual members. This information does change by random mutation, but the real driving force behind the evolutionary development is the combination and exchange of chromosomal material during breeding [Mitsuo Gen, Runwei Cheng, 1999]. In this book an optimization algorithm called winning particle optimization (WPO) is proposed [D.Micheli et, al,. 2010].

5.1 Winning particle optimization algorithm

Winning particle optimization (WPO), is a very simple algorithm, where at each time epoch of evolution, particle which best fit the objective function (OF), is deputed to pilot the trajectory of the remaining nonintelligent particles within the multidimensional space of solutions. In WPO, particles trajectories are simply defined by jumping of particles. Jumping is defined as coordinates sum or difference with respect to the current best fitting particle. The best particle represents the best position which defines the remaining particles search space and as a consequence, differently from the other particles, the best fitting

particle is not subject to any displacement action within the iteration cycle. It must remain in a fixed position while the other particles jump around it, searching for a new potential best position in the space of solutions. At each WPO iteration, a new portion of the search space is explored and the same or most probably a new potential better fitting location for each particle is always found. In Fig. 5.1.1, WPO flow chart related to (5.1.1) is shown. At the beginning of the algorithm, particles are randomly distributed within the *n*-dimensional search space. After that at the first step of the WPO algorithm, evaluation of objective function (OF) for all the particles are computed. In the next step, particles are compared to each other using value of their objective function and the best fitting particle is marked with its proper index position. Each particle position is completely defined by its coordinates and their number represents the dimensionality of the space where particles jump in search of the optimal final solution. Trajectory of each particle, except that of the best fitting particle, is defined in the following way: if m-th-coordinate position of a certain particle P^k is lesser then the corresponding m-th-coordinate position of the current best particle PB^q, then the new m-th-coordinate position will result from the sum of particle and best particle m-th-coordinates; while if m-th-coordinate position of a certain particle P^k is greater then the corresponding m-th-coordinate position of the current best particle PB^q, then the new m-th-coordinate position will result from the difference of best particle and particle m-th-coordinates;. Calling *q* the index of the best particle found at each iteration cycle, the condition which needs to be satisfied is $q \neq k$. Two different evolutions expressed by the Eq.(5.1.1) and (5.1.2), are possible, they define particles positions at *i+1*-th-iteration as a function of particles position at previous *i*-th-iteration. In the rest of work, method related to Eq.(5.1.2) has been applied.

$$P_m^k(i+1) = PB_m^q(i) + g \cdot \delta_m \cdot R_m \cdot P_m^k(i). \tag{5.1.1}$$

$$P_m^k(i+1) = \delta \cdot R_m \cdot P_m^k(i) + g \cdot PB_m^q(i) \tag{5.1.2}$$

where

$g = +1 \quad \text{if} \quad P_m^k(i) < PB_m^k(i)$

$g = -1 \quad \text{if} \quad P_m^k(i) > PB_m^k(i)$

$k = 1 \text{ to Particle Number}$

$q = 1 \text{ to Particle Number} \quad \text{and} \quad k \neq q$

$m = 1 \text{ to } n$

$n = \text{Space Dimensions}$

$R_m = \text{random number in the interval } [0 - 1]$

$\delta = \text{Convergenc eParameter}$

R is a random number in the closed range 0-1, which in random way adjust the amount of jumps for each single coordinate particle dimension. Such randomization helps the search phase of optimal solution. Convergence parameter δ is defined later; it helps the final convergence of the WPO algorithm. Even thought mutation operation has not been applied on the subsequent reported optimization it has to be noticed that mutation has been included in WPO algorithm. At the end of the WPO diagram, a boundary conditions check

for the new particles coordinates set is required in order to avoid to overcome the admitted constraints. The entire loop cycle can be iterated several times in order to get the required OF minimization.

When out of boundary conditions are verified for the *m*-th-particles coordinates, then, it could happen that some particles are forced to go toward the limit of search space.

During the evolution boundary conditions checking procedure is done and variables are set to *max* or *min* value of admitted range if the current value are respectively above or lower these limits. The WPO idea based on a quasi-random particles jumps system, assuring an effective method for solutions space exploration. In order to ease the WPO convergence, a mechanism which provide a progressive reduction of the maximum amplitude of jumps has been introduced and is identified by the triplet δ, P, σ parameters.

Calling *IN* the number of WPO iterations and supposing *i* the current *i*-th iteration, then the value of δ is given by the following equation:

$$\delta = \sigma \left(1 - \frac{i}{IN+1} \right)^P . \tag{5.1.3}$$

In (5.1.3), the meaning of σ, P parameters stays in fast or slow convergence of the WPO algorithm. In particular the higher the σ, the greater the initial jumps amplitude and the greater the distances where particles start to explore the search space. As far as *P* is concerned the higher its value, the faster the convergence to a suboptimal solution i.e., local minimum or maximum. The higher the current iteration number, the lower the δ parameter value. Parameter δ is by the position of the current particle, as in (5.1.1) and (5.1.2). Example related to (5.1.1) is::

$$P_m^k = BP_m^q + R_m \cdot P_m^k \cdot \delta \quad P_m^k = BP_m^q - R_m \cdot P_m^k \cdot \delta .$$

In Fig. 5.1.2, sequence of pictures shows the convergence of WPO algorithm for some canonical test functions [Franciszek Seredynski1, Albert Y. Zomaya, and Pascal Bouvry]: Sphere, Rastrigin, Griewank, Rosembrok, Akley, is shown. Parameter, is decreased with the iterations IN using $P = \sigma = 1$. Two different scenarios are compared, the first referring to Iteration Number (IN) = 500, Dimensions of Space Solution (DIM)=20, Number of exploring agents (Num Agents)=20; while the second referring to Iteration Number(IN)=500, Dimensions of Space Solution (DIM)=60, Number of exploring agents (Num Agents)=100.

In order to evaluate the robustness of WPO algorithm, for each test function, the algorithm as been tested repetitively for twenty times.

In Table. 5.1.1. and 5.1..2, the mean and standard deviation values are shown for two different scenario, the first referring to Iteration Number (IN)=500, Dimensions of Space Solution (DIM)=20, Number of exploring agents (Num Agents)=20; while the second referring to Iteration Number (IN)=500, Dimensions of Space Solution (DIM)=60, Number of exploring agents (Num Agents)=100.

It can be noticed that convergence difficulties increases for Rastrigin and Rosembrok test functions when the dimension of solution space changes from 20 to 60.
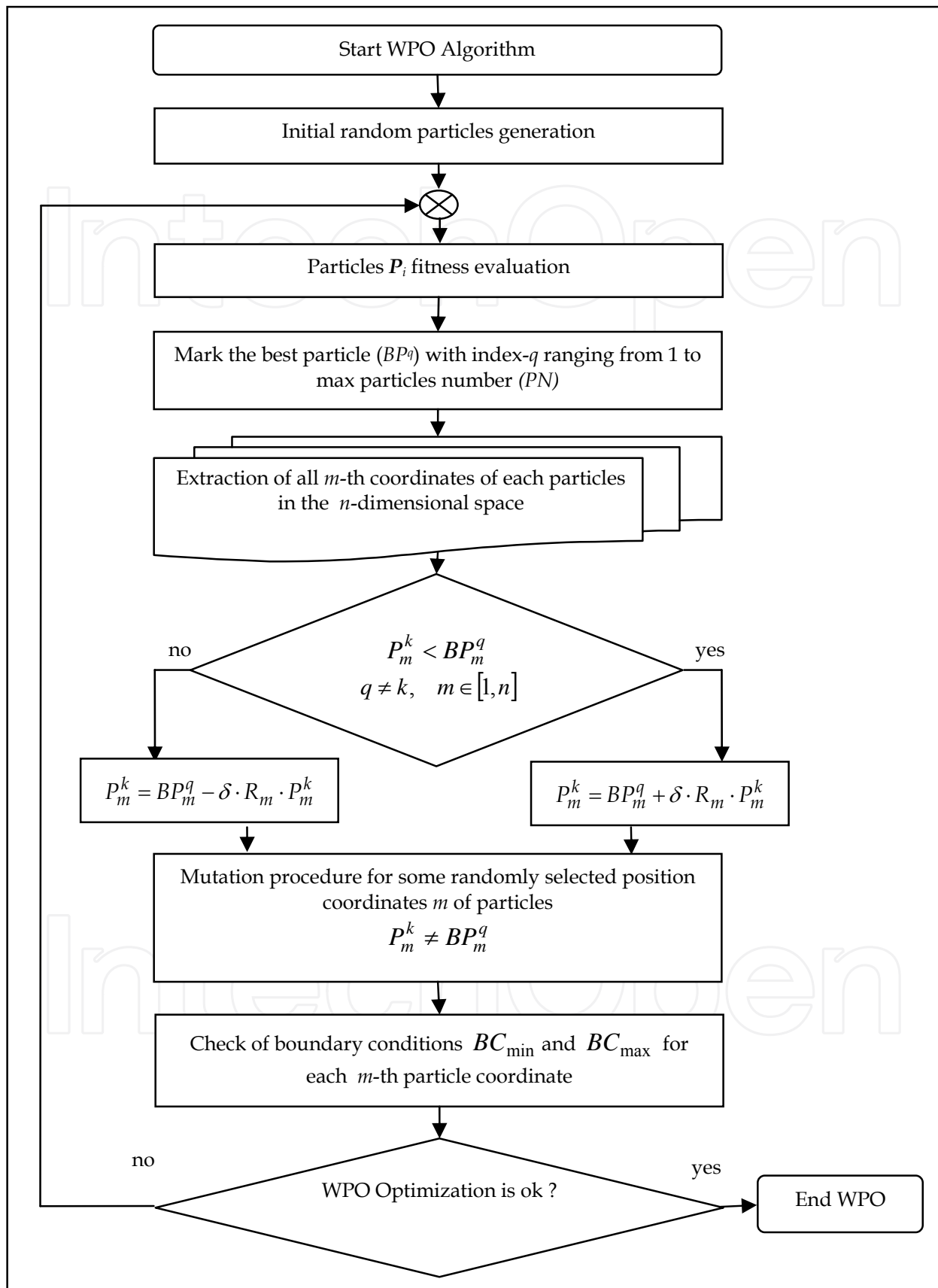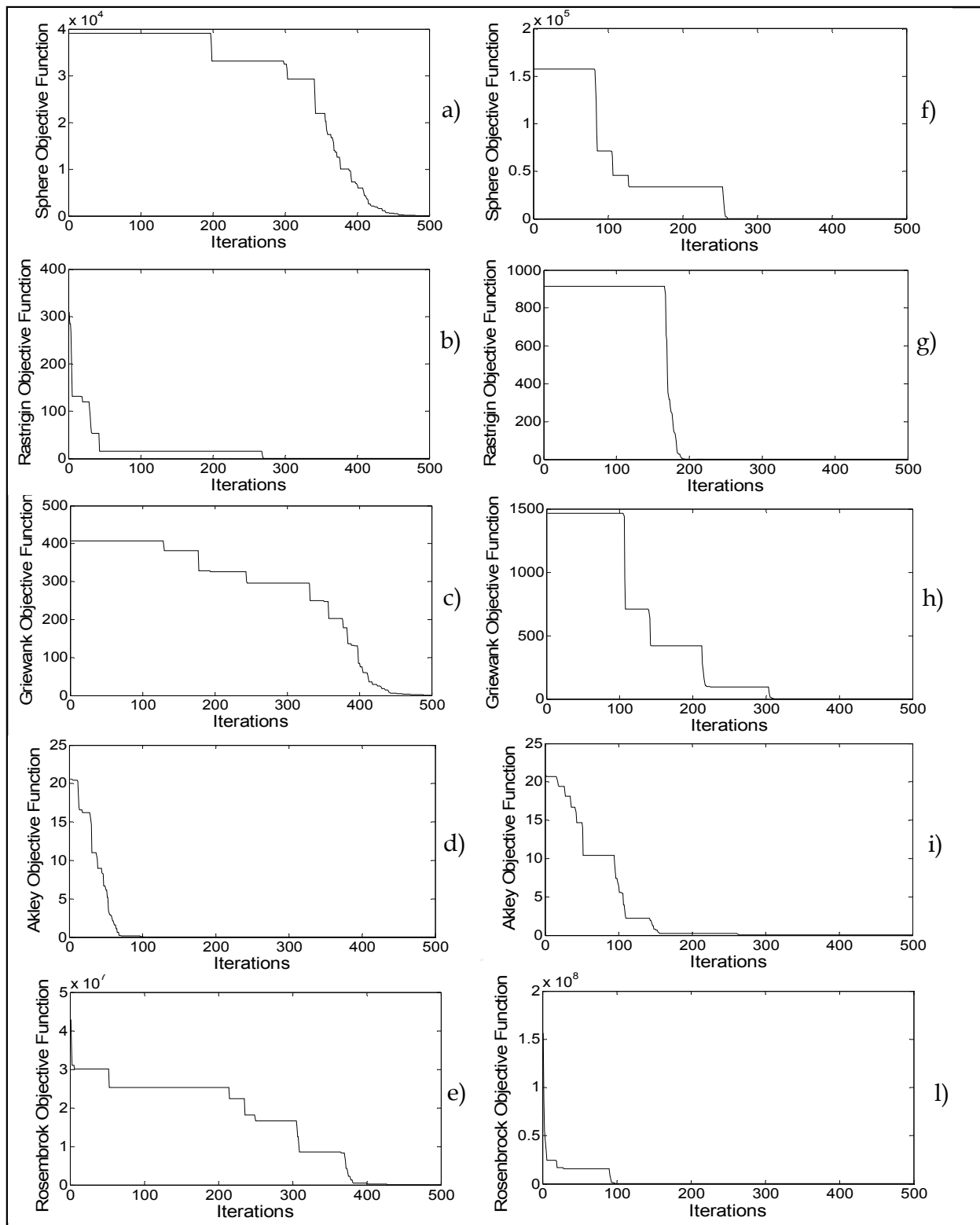
Fig. 5.1.1. WPO flow chart

Fig. 5.2.2. a),b),c),d),e) Typical Objective Function minimization with: IN=500, DIM=20, AGENT=20 and f),g),h),i),l) Typical Objective Function minimization with: IN=500, DIM=60, AGENT=100.

TEST Function	Theoretical Convergence value	WPO Mean Values Dim=20 NAgent=20	WPO Standard Deviation Dim=20 NAgent=20	WPO Mean Value Dim=60 NAgent=100	WPO Standard Deviation Dim=60 NAgent=100
Sphere	0	0	0	0	0
Rastrigin	0	0	0	0	0
Griewank	0	0	0	0	0
Rosenbrok	0	56.1	0.7	56.1	0.7
Akley	0	0	0	0	0

Table 5.1.1. WPO Test: IterNumber=500 , DIM=20 and 60, NumAgent=20 and 100, RunRipetition=20.

5.2 Absorber multilayer structure optimized by winning particle optimization

In Fig. 5.2.1, a design of an absorber in the 5-18 GHz band is shown. In particular the optimization has been conducted by the WPO algorithm, taking onto account for both: microwave loss factor maximization expressed in (4.2.1) and multilayer thickness minimization [D.Micheli et, al,. 2010]. In Fig. 5.2.1. a,b) reflection coefficient TE,TM remain below -10 dB for incidence angles in the range 0°-40° in the most part of the bandwidth (5.38-18 GHz).

In Fig. 5.2.1 b), it can be observed that for incidence angle of 20°, 30°, 40°, 60°, TM reflection coefficient is lower than that at 0° incidence angle. Such angles are the Brewster angles for a lossy material more often referred to Zenneck angles [Sophocles J.Orfanidis, 2009].

In Fig.5.2.1 c,d), transmission Coefficient TE, TM remain below -15 dB within all the bandwidth and linearly decrease with the frequency as expected.

In Fig.5.2.1. e) minimization of objective function is shown, it can be observed that after the 550 *i*-th iteration the convergence of WPO algorithm doesn't evolve towards lower values and as a consequence toward better solutions. In Fig. 5.2.1 f), the absorber multilayer structure is schematically shown. It can be observed two type of absorber mixed together the first where the intrinsic layer impedances decrease from the top to the bottom of absorber and the second where an high layer impedance (resin) is put between lower impedance layers (MWCNTs), recalling in mind resonant absorbers behaviour.

6. Experimental validation of mathematical model for microwave absorbers design

In order to experimentally validate the mathematical model and the design method described in previous sections, we realized and tested several multilayer square tiles, one made of graphite and the others made of MWCNTs. Tiles structure, their dimensions and reflection loss results (dB), are shown in Fig. 6.1.

In order to test the reflection loss of tiles we built an in-house NRL arch measurement, also called bi-static reflection method [Umari, M. H. et al.]. In this configuration, two antennas are used for transmitting and receiving signals respectively, and the microwave reflectivity at different incident angles can be measured. The NRL Arch is the industry standard for testing the reflectivity of materials. Originally designed at the Naval Research Laboratory
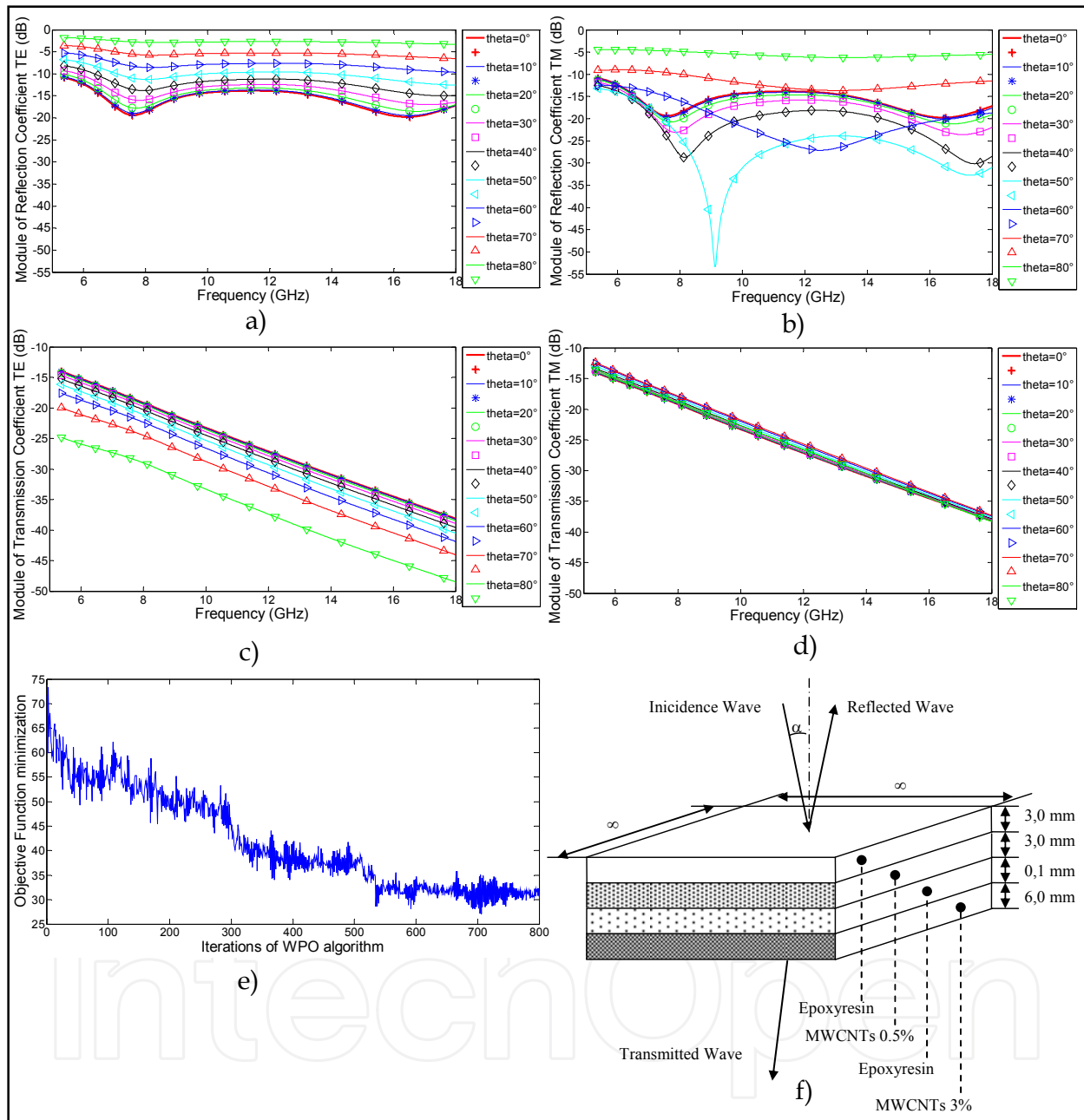
Fig. 5.2.1. a,b) Reflection coefficient (dB) TE, TM of absorber, c,d) Transmission coefficient (dB) TE, TM of absorber, e) WPO minimization of objective function which takes into account for both: loss factor and thickness, f) scheme of absorbing multilayer structure made of carbon composite material .
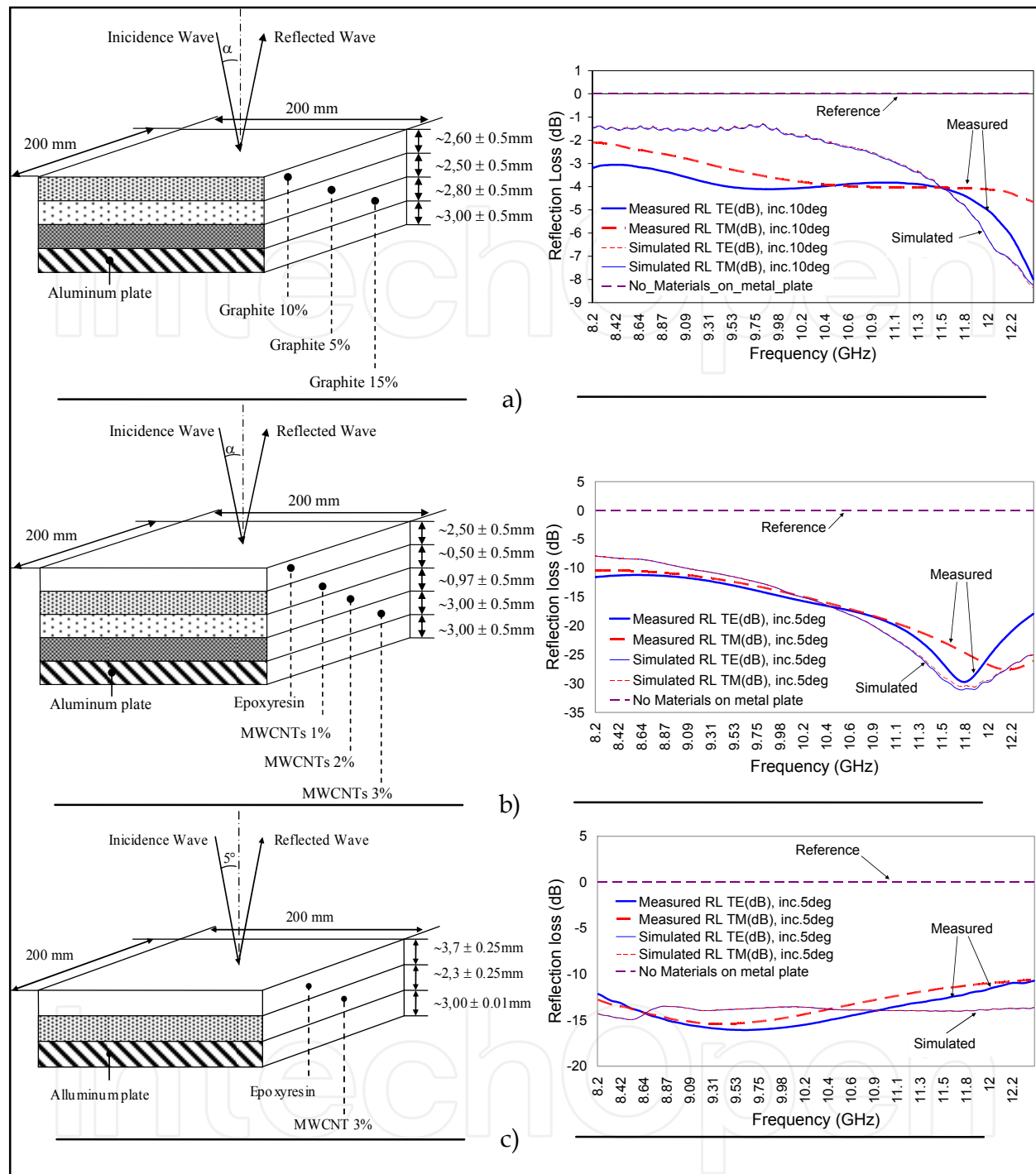
Fig. 6.1. a) Graphite based tile of 10.9 mm thickness; b) MWCNTs based tile of 6.97 mm thickness; b) MWCNTs based tile of 6 mm thickness.

(NRL), the NRL Arch allows for quick, repeatable and non-destructive testing of microwave absorbent materials over a wide frequency range. Reflectivity is defined as the reduction in reflected power caused by the introduction of an absorbent material. This reduction in power is compared to a '*perfect*' reflection which is approximated very well by the reflection of a flat metallic plate. Antennas can be located anywhere on the arch to allow measurements of performance at off normal angles of incidence. Vector network analyzer is

used for measurements to provide both the stimulus and the measurement. Calibration is performed by measuring the resultant power reflecting off the metal plate over a broad frequency range. This is established as the '*perfect*' reflection or 0 dB level (i.e. the reference level). The material under test is then placed on the plate and the reflected signal measured in dB. Time domain gating may be used to eliminate antenna cross talk and reduce the error introduced by room reflections. Using this configuration, the properties of materials at different directions can be characterized. It should be noted that in bi-static reflection measurements, the reflection is dependent on the polarization of the incident wave. Incident waves with parallel and perpendicular polarization usually result in different reflection coefficients. In Fig. 6.2, bistatic measurement system and the tiles in composite material are shown. In this configuration, bistatic measurement system has been based on Agilent software 8571E (material measurement), and Agilent PNA-L vector analyzer. Antennas were bought at Q-par Angus Ltd and are in the range 8-12 GHz. After calibration, measurement of a known sample consisting in ECCOSORB AN73 absorber, [www.eccosorb.com], has been performed in order to be aware about errors in the NRL measurement setup. Confidence of measurements was within 2 dB of interval with respect to reflection properties declared in ECCOSORB data sheet. At the end measurements of the manufactured samples have been performed for TE and TM mode. In Fig. 6.2, comparison between measured and simulated RAM structures is shown. It can be noticed that simulated curve shows similar behaviour with respect to measured one. Discrepancies in reflection loss data are around 2 dB, which is an acceptable accuracy in such kind of measurements.
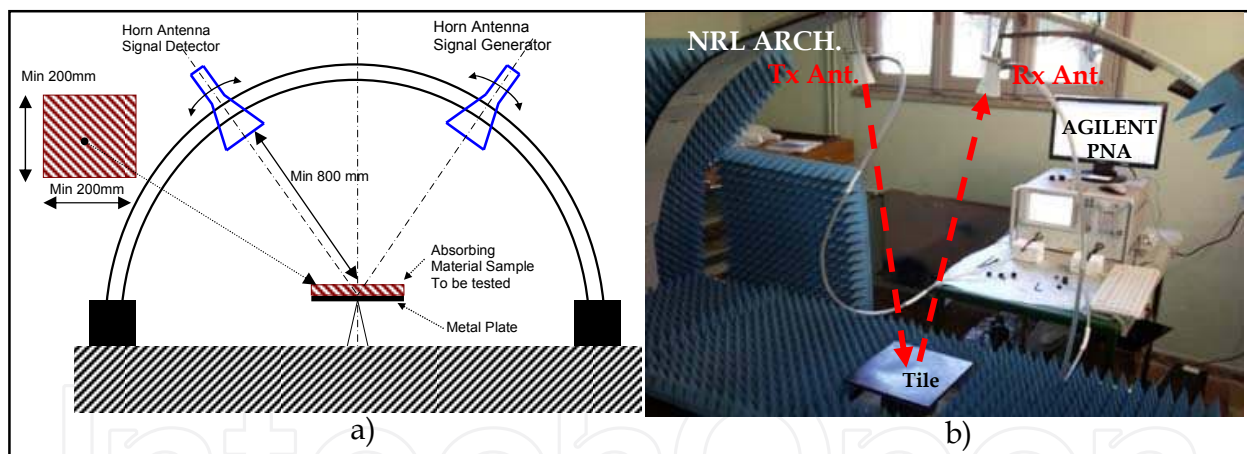

Fig. 6.2. a) bistatic measurement system sheme, b) bistatic measurement system located at (www.saslab.eu).

7. References

D. Micheli *, C. Apollo, R. Pastore, M. Marchetti, (2010). *X-Band microwave characterization of carbon-based nanocomposite material, absorption capability comparison and RAS design simulation*, Elsevier Composites Science and Technology 70 (2010) 400–409

Xingcun Colin Tong, (2009). *Advanced Materials and Design for Electromagnetic Interference Shielding*, CRC Press

Z. Ounaiesa,*, C. Parkb, K.E. Wiseb, E.J. Siochic, J.S. Harrisonc, (2003). *Electrical properties of single wall carbon nanotube reinforced polyimide composites*, Elsevier Science@Direct.

Weber, M, and Kamal., (1997). *Estimation of the volume resistivity of electrically conductive composites*, Polymer Composites 18(6), 711-725

Sichel, E., (1982). *Carbon Black-Polymer Composites*, New York: Marcel Dekker.

Prato et al.,(2008). *Using the Selective Functionalization of Metallic Single-Walled Carbon Nanotubes to Control Dielectrophoretic Mobility*. J. Am. Chem. Soc., 130 (25)

L. F.Chen and C. K. Ong, (2004). *Microwave Electronics; Measurement and Materials Characterization,* NeoNational University of Singapore Print & John Wiley

Abdel-Hakim and Boughriet, (1997). *Noniterative Stable Transmission/Reflection Method for Low-Loss Material Complex Permittivity Determination*, IEE Trans. Microwaves, Antennas Propagat., Vol. 45, N.1.

James Baker-Jarvis, (1990). *Transmission / Reflection and Short-Circuit Line Permittivity Measurements,* U.S. Department of Commerce, National Institute of Standard and Technology (NIST).

Davide M. Pozar, (2005). *Microwave Engineering*, John Wiley, third edition, pp. 174-180, 2005.

S. Ramo, J. Whinnery and T. Van Duzer, (1994). *Fields and Waves in Communications Electronics*, JohnWiley & Sons.

D. Micheli, R. Pastore, C. Apollo, M. Marchetti, G. Gradoni, F. Moglie, V. Mariani Primiani, (2009). *Carbon Based Nanomaterial Composites in RAM and Microwave Shielding Applications,* 9th Nanotechnology Conference: IEEE NANO 2009.

D. Micheli, R. Pastore, C. Apollo, M. Marchetti, G. Gradoni, F. Moglie, V. Mariani Primiani, (2010). *Design of Broadband Quasi-Perfect Electromagnetic Absorbers using Carbon Nanostructure-Based Composites*, IEEE Nanotechnology.

Davide Micheli, Carmelo Apollo, Roberto Pastore, Mario Marchetti, (2010). *Nanomaterials in Radar Absorbing Material Design using Particle Swarm Optimization and Genetic Algorithm*, 50th ISRAEL ANNUAL CONFERENCE ON AEROSPACE SCIENCES, Conference tag number: 50IACAS-542, Feb 2010.

Davide Micheli, Carmelo Apollo, Roberto Pastore, Mario Marchetti, (2010). *Modeling of Microwave Absorbing Structure using Winning Particle Optimization applied on Electrically Conductive Nanostructured composite material*, ICEM 2010 –XIX International Conference on Electrical Machines, TPC-6: Theory, Modeling and Design, Proc. IEEE. RF-013846, Set. 2010.

Mitsuo Gen, Runwei Cheng, (1999). *Genetic Algorithms, 1st edition,* John Wiley & Sons.

Franciszek Seredynski1, Albert Y. Zomaya, and Pascal Bouvry. *Function Optimization with Coevolutionary Algorithms.*

Umari, M. H. Ghodgaonkar, D. K. Varadan, V. V. and Varadan, V. K. (1991). *A free-space bistatic calibration technique for the measurement of parallel and perpendicular reflection coefficients of planar samples*, IEEE Transactions on Instrumentation and Measurement, 40 (1), 19–24.

Emerson & Cuming Microwave Products. *NRL Arch Reflectivity Testing basic notes*. Available: http://www.eccosorb.com/

Sophocles J.Orfanidis, (2009). *Electromagnetic wave and Antennas.*
        http://www.ece.rutgers.edu/
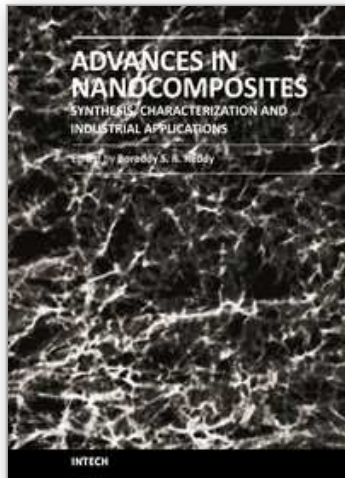
Advances in Nanocomposites - Synthesis, Characterization and Industrial Applications

Edited by Dr. Boreddy Reddy

Advances in Nanocomposites - Synthesis, Characterization and Industrial Applications was conceived as a comprehensive reference volume on various aspects of functional nanocomposites for engineering technologies. The term functional nanocomposites signifies a wide area of polymer/material science and engineering, involving the design, synthesis and study of nanocomposites of increasing structural sophistication and complexity useful for a wide range of chemical, physicochemical and biological/biomedical processes. "Emerging technologies" are also broadly understood to include new technological developments, beginning at the forefront of conventional industrial practices and extending into anticipated and speculative industries of the future. The scope of the present book on nanocomposites and applications extends far beyond emerging technologies. This book presents 40 chapters organized in four parts systematically providing a wealth of new ideas in design, synthesis and study of sophisticated nanocomposite structures.

How to reference

In order to correctly reference this scholarly work, feel free to copy and paste the following:

Davide Micheli, Carmelo Apollo, Roberto Pastore, Ramon Bueno Morles, Mario Marchetti and Gabriele Gradoni (2011). Electromagnetic Characterization of Composite Materials and Microwave Absorbing Modeling, Advances in Nanocomposites - Synthesis, Characterization and Industrial Applications, Dr. Boreddy Reddy (Ed.), ISBN: 978-953-307-165-7, InTech, Available from: http://www.intechopen.com/books/advances-in-nanocomposites-synthesis-characterization-and-industrial-applications/electromagnetic-characterization-of-composite-materials-and-microwave-absorbing-modeling

INTECH

open science | open minds